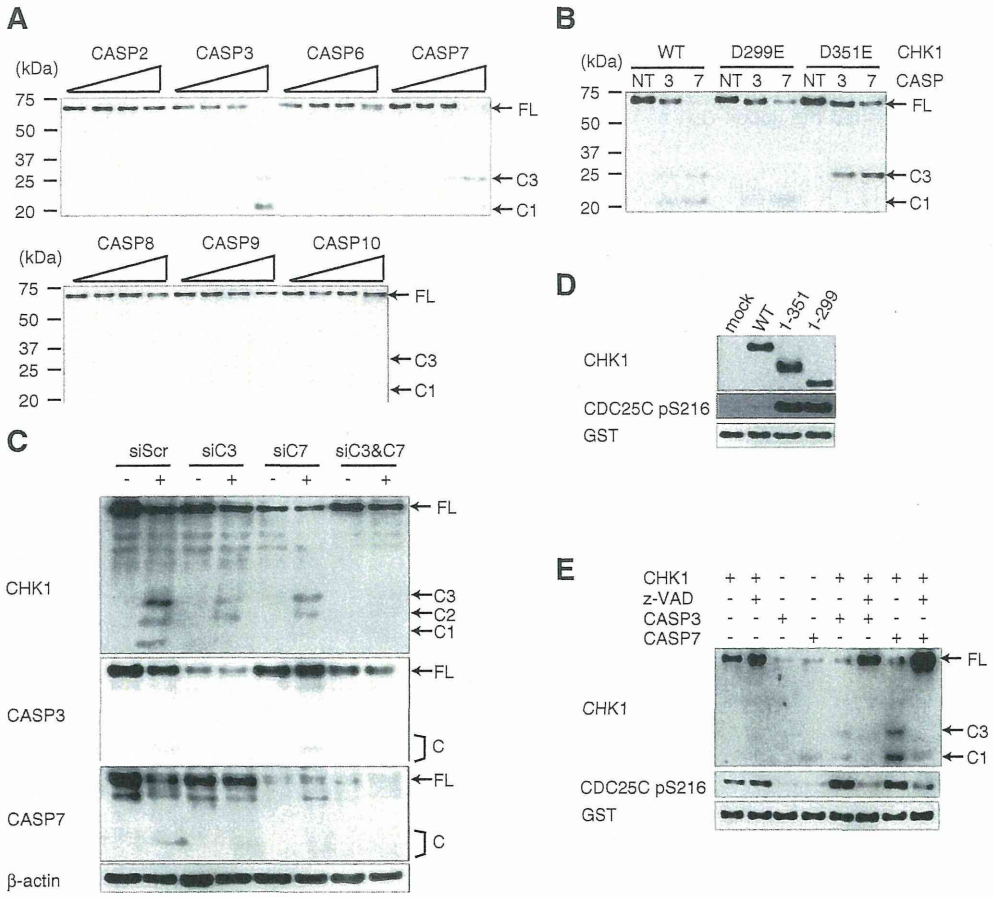

Fig. 2. Identification of CASP family proteases responsible for CHK1 cleavage and the effect of cleavage on CHK1 kinase activity. (A) Recombinant 3× FLAG-CHK1–3× Myc was incubated with apoptosis-related CASP2, CASP3, CASP6, CASP7, CASP8, CASP9, or CASP10 for 24 h at 37 °C. CHK1 cleavage was analyzed by western blotting using anti-Myc-Tag antibody. (B) Recombinant 3× FLAG-CHK1–3× Myc (CHK1 WT, D299E or D351) was incubated with CASP3 or CASP7 for 24 h at 37 °C. CHK1 cleavage was analyzed by western blotting using anti-Myc-Tag antibody. (C) U2OS cells were transfected with 10 nM siRNAs against GFP (siScr), CASP3 (siC3), CASP7 (siC7), or siC3 and siC7 for 24 h, and then treated with 100 μM ETP for 48 h. CHK1 cleavage was analyzed by western blotting using the indicated antibodies. (D) In vitro translated full-length CHK1 (WT) or truncated forms of CHK1(1–299, 1–351) were incubated with GST-CDC25C at 30 °C for 30 min. CHK1 kinase activity was analyzed by Western blotting with anti-CDC25C (pSer216). (E) Recombinant CHK1 was pre-incubated with or without CASP3, CASP7, at 37 °C for 8 h in the presence or absence of 100 μM zVAD-fmk. CHK1 was then incubated with GST-CDC25C at 30 °C for 30 min, and analyzed by Western blotting with the indicated antibodies.

siRNA-mediated knockdown of CASP3 or CASP7 inhibits CHK1 cleavage in DNA damage-induced PCD. As shown in Fig. 2C, knockdown of CASP3, CASP7, or both CASP3 and CASP7 inhibited CHK1 cleavage. These results show that CASP3 and CASP7 are responsible for CHK1 cleavage at both D^{299} and D^{351}.

We subsequently performed CHK1 kinase assays to evaluate cleaved CHK1 kinase activity. Since CHK1 has an auto-inhibitory region at its C-terminus [24–27], we estimated that CHK1 cleavage has the potential to elevate its kinase activity. In this study, we used an assay that detects CDC25C phosphorylation by Western blotting with an anti-CDC25C(phospho-S^{216}) probe [18]. We first prepared full-length, CHK1(FL), and cleavage forms of CHK1 containing the relevant kinase domain, CHK1(1–299) and CHK1(1–351). As shown in Fig. 2D, kinase activities of both CHK1(1–299) and CHK1(1–351) drastically increased in comparison to that of CHK1(FL). This observation is consistent with past studies that found that deletion of the C-terminus of CHK1 enhances its kinase activity [15,24–27]. Next, we tested whether the activity of the CASP-cleaved CHK1 containing the kinase domain fragment and auto-inhibitory region was elevated. Recombinant CHK1(FL) pre-incubated with or without CASP3 or CASP7 in the presence or absence of 100 μM zVAD-fmk was subjected to the CHK1 kinase assay (Fig. 2E). The kinase activity of CHK1 pre-incubated with CASP3 or CASP7 was elevated in comparison to that of pre-incubated CHK1 alone, and the elevation was inhibited by co-pretreatment with z-VAD. These results show that the cleavage of CHK1 by CASP3 or CASP7 elevates its kinase activity.

3.3. Identification of a recognition sequence associated with non-CASP family proteases in CHK1 cleavage

From the results of Fig. 2A, we noticed that none of the apoptotic CASP proteases induced production of a C2 fragment. Since this result raised the possibility that non-CASP family proteases are involved in N2–C2 cleavage, we performed further analyses of the recognition sequence. Previously, it has been reported that the P1 residue in the CASP recognition sequence is an aspartic acid residue [3–5]. This implies that if N2–C2 cleavage is catalyzed by the CASP family, a mutation of the P1 residue would result in inhibition of cleavage. Therefore, we sought to identify the recognition sequence of N2–C2 cleavage by using site-directed mutagenesis involving mutation of aspartic acid to glutamic acid. Considering the molecular weights of the cleavage products (Fig. 1), we explored aspartic acid residues in the surrounding amino acid sequences and found aspartic acid residues at positions 258, 262, 299, 329, 336, 351, 385, and 387 (Fig. 3A). Next, we constructed plasmid vectors harboring a wild-type or an aspartic acid-to-glutamic acid substitution mutant of CHK1 with a Flag-tag at the N-terminus and a Myc-tag at the C-terminus. After induction of PCD in U2OS cells that had been

transfected with each vector, the C-terminal fragments of CHK1 were analyzed by Western blotting with anti-Myc (Fig. 3B). Although D299E and D351E mutation inhibited production of C3 and C1, respectively, we could not identify any mutation that inhibited production of C2. This result supported the notion that non-CASP family proteases are involved in N2–C2 cleavage. Next, to identify the recognition sequence associated with the non-CASP family proteases (termed as seq-X), we devised a strategy to narrow down the identification of seq-X by using C- or N-terminal deletion mutants (Fig. 3C). Firstly, for detection of cleaved products, C-terminal and N-terminal

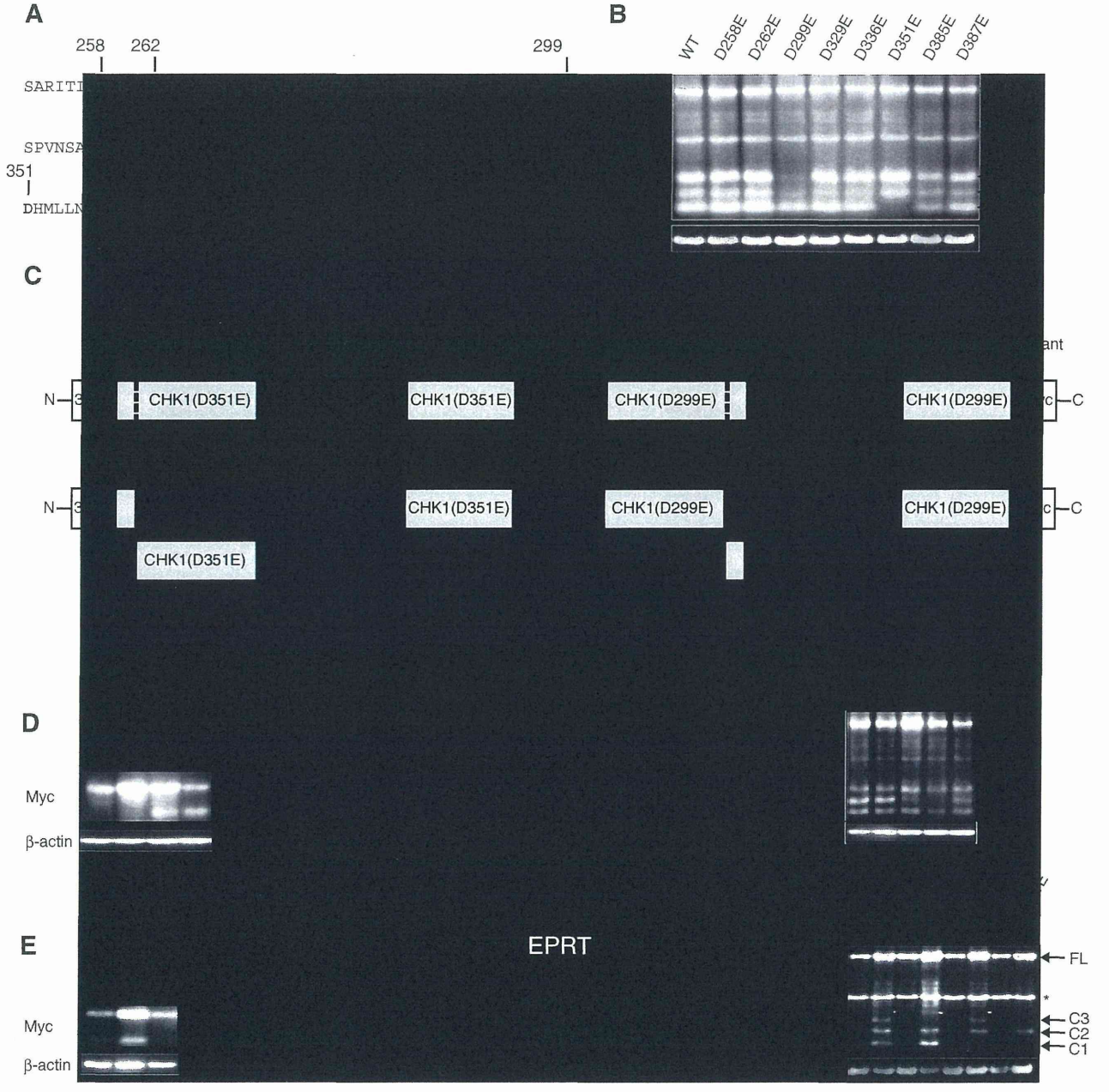

Fig. 3. Identification of a recognition sequence associated with non-CASP family proteases in CHK1 cleavage. (A) CHK1 amino acid sequences between position 251 and position 410 are shown. Bold letters represent aspartic acid residues. (B) A plasmid vector harboring a wild-type CHK1 or a glutamic acid substitution CHK1 mutant form of D^{258}, D^{262}, D^{299}, D^{329}, D^{336}, D^{351}, D^{385}, or D^{387} was transfected into U2OS cells. The cells were treated with 100 μM Etp for 36 h, and the cleaved C-terminal fragments of CHK1s were analyzed by Western blotting with anti-Myc. The asterisk indicates a non-specific band. (C) Strategy for identification of recognition sequences for cleavage at seq-X. N-terminal and C-terminal deletion mutants were fused to 3× Myc at the N-terminal and C-terminal, respectively. For cleavage at only seq-X, D^{299} in each C-terminal deletion mutant and D^{351} in each N-terminal deletion mutant were mutated to alanine. After PCD induction, only mutants possessing the recognition sequences were cleaved into two fragments as shown. (D and E) U2OS cells were transfected with expression vectors encoding the indicated N-terminal (D) or C-terminal (E) deletion mutants. After 36 h of transfection, the cells were treated with 100 μM Etp for 48 h. (F) The recognition sequences for cleavage at seq-X were estimated from the data presented in panels D and E. The asterisk indicates a non-specific band. (G) A plasmid vector harboring a wild-type CHK1 or an alanine substitution CHK1 mutant form of E^{320}, P^{321}, R^{322}, or T^{323} was transfected into U2OS cells. The cells were treated with 100 μM Etp for 36 h, and the C-terminal fragments of CHK1s were analyzed by Western blotting with anti-Myc. (H) A plasmid vector harboring a wild-type CHK1 or a glutamic acid substitution CHK1 mutant form of D^{299}, D^{351}, or D^{299} and D^{351} was transfected into U2OS cells. The cells were treated with 2 μM LLnV for 36 h, and the cleaved C-terminal fragments of CHK1s were analyzed by Western blotting with anti-Myc. The asterisk indicates a non-specific band.

deletion mutants were fused to 3× Myc at the C-terminus and N-terminus, respectively. Secondly, for detection of products cleaved at only seq-X but not other identified sequences, D^{299} in each C-terminal deletion mutant and D^{351} in each N-terminal deletion mutant were mutated to glutamic acid. By this strategy, it is likely that after PCD induction, only mutants possessing seq-X are cleaved into two fragments and the smaller products fused to 3× Myc tag are detected by Western blotting with anti-Myc antibody. Because preliminary analyses using N-terminal deletion mutants (311–476, 316–476, and 321–476 mutants) and C-terminal deletion mutants (1–318, 1–320, 1–322, and 1–324 mutants) suggested that the putative seq-X is located between positions 319 and 324 (data not shown), we further analyzed using four C-terminal deletion mutants (1–321, 1–322, 1–323, and 1–324) and three N-terminal deletion mutants (319–476, 320–476, and 321–476). As shown in Fig. 3D, in N-terminal deletion series, the 321–476 mutant was not cleaved. As shown in Fig. 3E, In the C-terminal deletion series, the 1–321 and 1–322 mutants were not cleaved. These results show that the seq-X is ^{320}EPRT^{323} or, in other words, that it is not a CASP consensus sequence (Fig. 3F), suggesting that the "EPRT proteases" in question are non-CASP family proteases. Furthermore, we confirmed whether alanine mutations of these sequences affect cleavage. As shown in Fig. 3G, P321A and R322A mutation, but not E320A and T323A mutation, efficiently inhibited production of the C2 fragment. Moreover, the inhibition of EPRT cleavage by site-directed mutagenesis did not affect either D^{299} or D^{351} cleavage. We also analyzed whether the mutation of sites cleaved by CASP affect EPRT cleavage (Fig. 3H). The mutation of D^{299} and/or D^{351} cleavage did not significantly affect EPRT cleavage. Taken together, these results indicate that CHK1 cleavage by CASP and non-CASP can occur independently of each other.

3.4. PCD induction at a specific cell cycle phase and CHK1 cleavage

Considering that CHK1 is involved in cell cycle regulation, we explored the relationship between PCD at a specific cell cycle phase and CHK1 cleavage, using DNA damaging agents. We chose to use Cis, a direct DNA crosslinker as a PCD inducer. Indirect DNA damaging agents such as Cpt and Etp, for example, were not appropriate for our purposes, because their pharmacological effects are dependent on cell cycle phases. First, using the DTB method, G1/S-boundary, S, G2, or G1 phase-enriched cells were prepared and then induced to PCD by treatment with Cis (Fig. 4A). PCD induction of G1 phase-enriched cells induced a CHK1 cleavage profile that was different to the profiles induced by PCD induction of cells enriched from the other phases. The cleavage products (both N- and C-terminus) from ^{320}EPRT^{323} markedly increased compared with those from D^{299} and D^{351} (Fig. 4B). Using a marker of apoptosis, PARP1 cleavage, it was apparent that the induction efficiency of PCD in G1/S or G1 phase-enriched cells was higher than that of S and G2 phase-enriched cells. To exclude the possibility that these findings result from an artifact of the DTB method, we confirmed the finding by using cells synchronized by the TNB method. By this method, M, G1, or S phase-enriched cells were prepared and then treated with Cis to induce PCD (Fig. 4C). As shown in Fig. 4D, PCD induction of cells enriched from G1 phase, but not M and S phases, caused increased cleavage at ^{320}EPRT^{323}. Furthermore, from the results of PARP1 cleavage and CASP3 activation, the efficiency of PCD induction in M or G1 phase-enriched cells was higher than that of S phase-enriched cells. These results indicate that CHK1 cleavage, when inducing PCD at G1 phase, is different from that of the other phases.

4. Discussion

In this study, we showed the intricate regulatory mechanisms of CHK1 cleavage during PCD (Fig. 5). Firstly, we showed that CHK1 cleavage efficiently occurs in PCD induced by DNA damaging agents such as Cis, Cpt, and Etp, as well as cathepsin, calpain, and proteasome inhibitors such as LLnV and LLnL (Fig. 1B and 1C). DNA damage-induced PCD led to increases in protein levels of cleaved CHK1 and decreases in protein levels of full-length CHK1. On the other hand, LLnV and LLnL-induced PCD led to increases in protein levels of cleaved CHK1 without any significant decrease in full-length CHK1. Considering that ubiquitin–proteasome pathway is involved in turnover of CHK1 protein [28–30], the increases of total CHK1 protein may spoil the decreases in the protein levels of full-length CHK1 induced by PCD. Next, we showed that both CASP and a specific serine protease family regulate CHK1 cleavage. Interestingly, serine protease inhibitors efficiently inhibited CHK1 cleavage and slightly inhibited PARP1 cleavage (Fig. 1D). Considering that PARP1 is cleaved by CASP3 and CASP7 as well as CHK1 [31,32], these results means that although the CASP3 or CASP7-mediated PCD pathway were still active, CHK1 cleavage was completely inhibited. Hence, CASPs activation is essential but not sufficient for CHK1 cleavage. It may be that the serine proteases are required for changing CHK1 to a "cleavable state" (for example, elimination of endogenous CHK1 cleavage inhibitor) rather than cleaving CHK1 directly. In any case, our results indicate that even if PCD is CASP independent, CASP activation would be required for CHK1 cleavage. Furthermore, we demonstrated that one candidate serine protease involved in CHK1 cleavage is HTRA2. It is known that HTRA2 enhances both CASP-dependent and CASP-independent PCD pathways [33]. Consistent with this result, serine protease inhibitor treatment slightly inhibited the activation of some apoptotic CASPs in DNA damage-induced PCD (data not shown). Considering that CASP3 and CASP7 are activated even under serine protease inhibition, HTRA2 may contribute to CHK1 cleavage in a CASP-independent manner. Interestingly, we noticed that even in the absence of Etp or LLnV treatment, HTRA2 inhibition by siRNA-mediated gene knockdown or chemical inhibition elevated the CHK1 protein levels (Fig. 1E and F). This result may imply the physiological interaction between HTRA2 and CHK1. To address whether only HTRA2 contributes to CHK1 cleavage as the serine protease, HTRA2 deficient cells would be required.

Our results suggest that CHK1 cleavage is directly executed by CASP3, CASP7, and as yet unidentified non-CASP family proteases, and that CHK1 cleavage by CASP and non-CASP can occur independently of each other (Figs. 2 and 3). As shown in Fig. 2A, we obtained in vitro data that both CASP3 and CASP7 cleave CHK1 at both D^{299} and D^{351}, and none of the apoptotic CASPs cleave CHK1 by recognizing ^{320}EPRT^{323}(Fig. 3C–G). Taken together with the fact that EPRT is not a CASP consensus recognition sequence, our results strongly suggest that the unidentified protease is not a member of the CASP family. While the truncation analysis suggests that ^{320}EPRT^{323} is the recognition sequence, P321A and R322A mutation, but not E320A and T323A mutation, efficiently inhibited ^{320}EPRT^{323} cleavage (Fig. 3C–G). Hence, mutation analyses other than Ala would be required to determine the essential amino acid residue(s) in the ^{320}EPRT^{323} cleavage. We suspected the involvement of lysosomal proteases such as the cathepsin family in ^{320}EPRT^{323} cleavage, because lysosomes are reportedly involved in apoptotic cell death [34]. The inhibition of Cathepsin B, D, G, or L by chemical compounds [34–37], which are involved in certain types of PCD [38], did not inhibit all instances of CHK1 cleavage (data not shown). In addition, the inhibition of pH-dependent lysosomal proteases by bafilomycin A1 [35] did not affect CHK1 cleavages (data not shown). These results indicate that proteases other than those described above would contribute to CHK1 cleavages. Moreover, we obtained data that, under conditions whereby calpains, cathepsins, and proteasomes are inhibited, CHK1 cleavage can occur (Fig. 1C). The fact that siRNA-mediated knockdown of CASP3 and/or CASP7, and z-VAD-fmk treatment, inhibit EPRT cleavage suggests that EPRT protease(s) is also regulated by the CASP pathway (Fig. 2C). We are currently exploring candidate proteases of ^{320}EPRT^{323} cleavage. Furthermore, in the induction of PCD in cell cycle-synchronized cells, we obtained the interesting

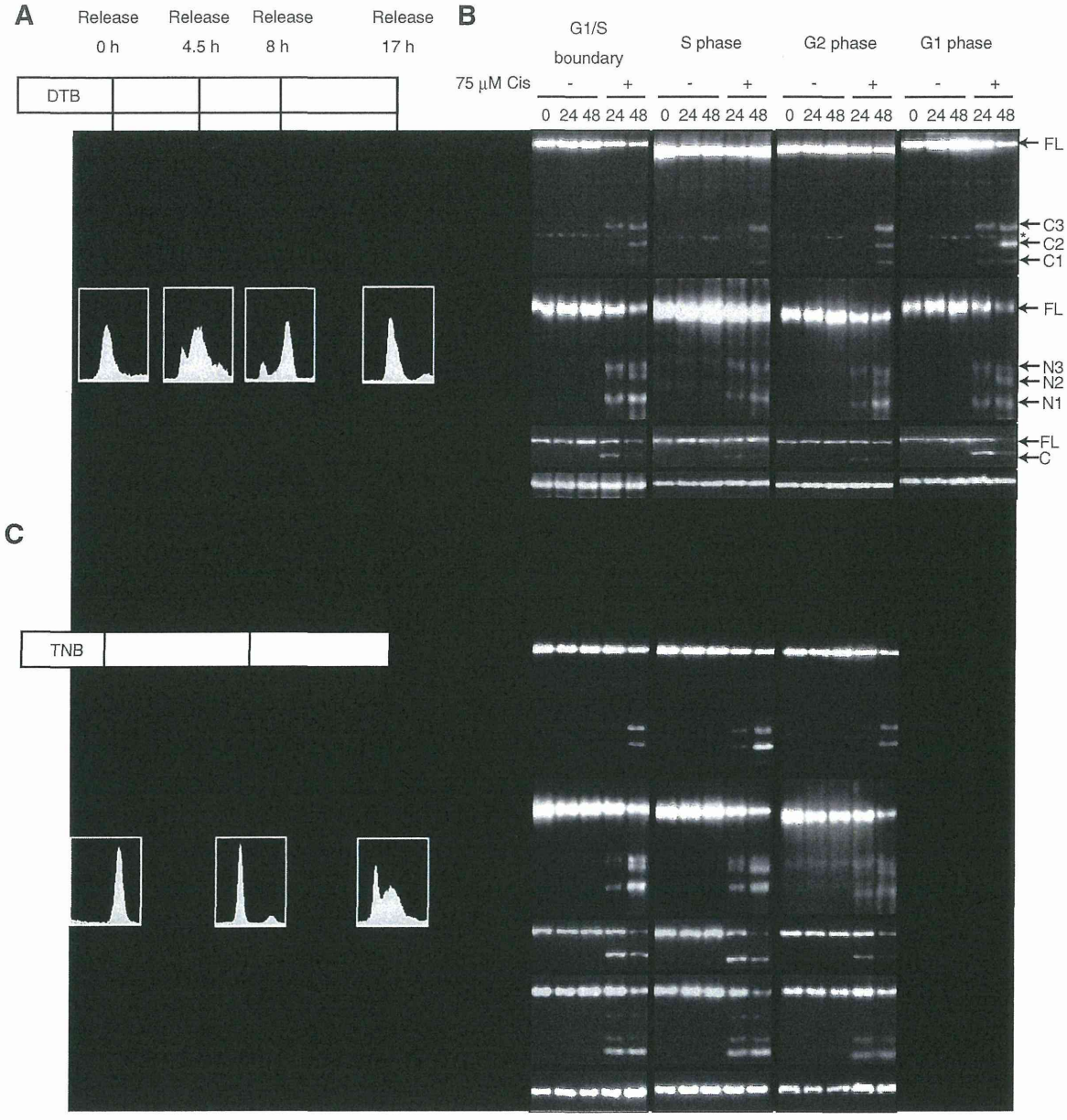

Fig. 4. Enhancement of CHK1 cleavage by EPRT protease in PCD induction at a specific cell cycle phases. (A and C) Procedures for analysis of the cell cycle specificity of CHK1 cleavage. (B) U2OS cells synchronized at G1, G1/S, S, or G2 phase by DTB method were treated with 75 μM of Cis and the cell extracts were analyzed by Western blotting with the indicated antibodies. (D) U2OS cells synchronized at M, G1, or S (right) phase by TNB methods were treated with 75 μM of Cis and the cell extracts were analyzed by Western blotting with the indicated antibodies. The asterisk indicates a non-specific band.

observation that ^{320}EPRT^{323} cleavage of CHK1 occurs efficiently in PCD, which is induced at the G1 phase (Fig. 4). On the other hand, we did not observe a cell cycle phase preference for D^{299} and D^{351} cleavage. We suggest two possibilities that may explain this cell cycle-related difference in ^{320}EPRT^{323} cleavage. The first possibility is that EPRT proteases may be activated and/or up-regulated at G1 phase. Currently, we do not know any PCD-related proteases that are regulated in a cell cycle phase-specific manner. However, considering the existence of cell cycle-selective PCD such as mitotic catastrophe [1,2], such proteases may exist. The second possibility is that post-transcriptional modification of CHK1 may increase the efficiency of ^{320}EPRT^{323} cleavage. A previous study has reported that cleavage-site phosphorylation is disadvantageous with respect to cleavability by CASPs [39]. We are interested in the relationship between post-transcriptional modifications of CHK1 and effects on CHK1 cleavage. Our group and another have already confirmed that S^{317} and S^{345} phosphorylations, which are well known as DNA damage-responsive phosphorylation sites, do not critically affect CHK1 cleavage during PCD (data not shown, 15). Furthermore, in PCD in G1 phase-enriched cells, since the CASP-cleaved sites D^{299} and D^{35} are also cleaved, the physiological significance appears to not be simple as the EPRT cleavage compensates for D^{299} and/or D^{351} cleavage. It remains unclear whether the preferential cleavage of ^{320}EPRT^{323} at G1 phase contributes to the regulation of cell cycle-selective PCD, directly or indirectly.

We found that CHK1 cleavage leads to elevated kinase activity (Fig. 2D and E). Although the data presented here indicate that CASP3 and CASP7-mediated cleavage elevates CHK1 kinase activity, we were not able to address the effect on kinase activity by ^{320}EPRT^{323} protease-mediated cleavage because the position of amide bonds cleaved by ^{320}EPRT^{323} proteases has been not identified. Nevertheless,

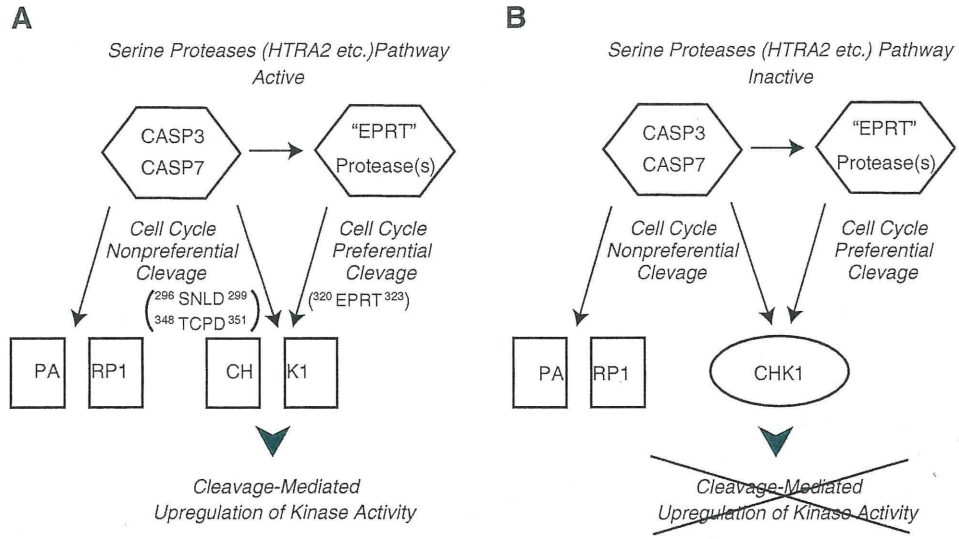

Fig. 5. A model of CHK1 cleavage regulation during PCD. The PCD signal activates certain types of serine proteases such as HTRA2 as well as the CASP family. The serine protease(s)-involved pathway alters CHK1 to the cleavable state. Therefore, under conditions where the serine protease(s) is active, CHK1 is cleaved by CASP3 and CASP7 at ^{296}SNLD^{299} and ^{348}351 in a cell cycle-nonpreferential manner, and by unidentified EPRT proteases at ^{320}EPRT^{323} in a cell cycle-preferential manner, which results in elevated kinase activity (A). On the other hand, under conditions where the serine protease(s) is inactive, CHK1 is not cleaved (B). PARP1 is cleaved by CASP3 and CASP7 without critical involvement of the serine protease pathway.

we anticipate that CHK1 cleavage by ^{320}EPRT^{323} proteases would induce up-regulation of its kinase activity as well as that by CASPs. The basis for this prediction is as follows: i) The auto-inhibitory region of CHK1 is located at approximately 100 amino acids from its C-terminus (full-length CHK1; 476 amino acids) [24–27], ii) ^{320}EPRT^{323} lies between ^{296}SNLD^{299} and ^{348}TCPD^{351} (Fig. 3), iii) the kinase activity of CHK1(1–299) and CHK1(1–351) increases compared with that of full-length CHK1 (Fig. 2), and iv) the kinase activity of CHK1(1–308) and CHK1(1–335) increases compared with that of full-length CHK1 [26]. The most important question is how PCD-specific CHK1 activation affects PCD. The regulation of CHK1 cleavage may be a secondary event in PCD because, as shown in Fig. 2, CHK1 cleavage requires CASP3 and CASP7 activation, which generally occur after loss of mitochondrial membrane potential [1,2]. Considering that CHK1 inhibits cell cycle progression in response to DNA damage, cell cycle progression should already be arrested prior to the execution of DNA damage-induced PCD. Therefore the cleavage-mediated CHK1 activation may contribute to shutdown the cell cycle machinery or to afford more efficient processing of cellular components during PCD. To clarify this question would require investigation of the differences of binding partners or substrate specificity between full-length CHK1 and cleaved CHK1.

It has been reported that previously identified "death substrates involved in DNA damage response" are cleaved or regulated by CASP [7–13]. On the other hand, CHK1 cleavage is involved in multiple protease families (serine protease, CASP, and unidentified EPRT protease family). These findings may imply that CHK1 cleavage plays an important role in DNA damage-induced PCD, or that "death substrate cleavage" itself may involve more complicated mechanisms than previously thought. In any case, the contribution of CHK1 cleavage to PCD is not likely to be simple. To study the contribution of CHK1 cleavage to PCD via these intricate regulatory mechanisms, requires not only the identification of proteases involved in CHK cleavage but also lethality and the processes of various types of PCD. Furthermore to clarify the physiological roles of CHK1 cleavage, requires evaluation of whether the inhibition of all CHK1 cleavages and subsequent changes of kinase activity affect PCD. We are constructing cells that stably express mutants that are kinase active and uncleavable and kinase inactive and uncleavable. By using these cells, we will evaluate the effects of CHK1 cleavage on PCD by coordinating various viewpoints such as ATP/NAD$^+$ levels, chromatin condensation, mitochondrial outer membrane potential, membrane blebbing, and so on. In summary, our results shed light on the complexity of PCD-mediated protein cleavage and cell cycle-specific regulation of the PCD pathway. CHK1 cleavage may provide a useful model to show the complexity involved in this regulation.

Supplementary data to this article can be found online at http://dx.doi.org/10.1016/j.bbagen.2012.10.009.

Acknowledgements

We thank Dr. Jun-ichi Sakai, Mr. Akihiko Mizoroki, Mr. Toru Sakagami, and Ms. Kikumi Yoshida (Tokyo University of Science, Japan) for their technical assistance; and all members of Tanuma and Higami laboratories for their cooperation. The first author also thanks Machiko Okita and Soju Okita for their valuable encouragement. This work was supported by a Research Grant for Promoting Technological Seeds (A) from the Japan Science and Technology Agency (N.O.) and a Research Grant for Young Scientists from Tokyo University of Science (N.O.) and partially by a Grant-in-Aid for Young Scientists (B) (23790201) from the Ministry of Education, Culture, Sports, Science and Technology (N.O.).

References

[1] G. Kroemer, L. Galluzzi, P. Vandenabeele, J. Abrams, E.S. Alnemri, E.H. Baehrecke, M.V. Blagosklonny, W.S. El-Deiry, P. Golstein, D.R. Green, M. Hengartner, R.A. Knight, S. Kumar, S.A. Lipton, W. Malorni, G. Nuñez, M.E. Peter, J. Tschopp, J. Yuan, M. Piacentini, B. Zhivotovsky, G. Melino, Classification of cell death: recommendations of the Nomenclature Committee on Cell Death 2009, Cell Death Differ. 16 (2009) 3–11.

[2] L. Galluzzi, I. Vitale, J.M. Abrams, E.S. Alnemri, E.H. Baehrecke, M.V. Blagosklonny, T.M. Dawson, V.L. Dawson, W.S. El-Deiry, S. Fulda, E. Gottlieb, D.R. Green, M.O. Hengartner, O. Kepp, R.A. Knight, S. Kumar, S.A. Lipton, X. Lu, F. Madeo, W. Malorni, P. Mehlen, G. Nuñez, M.E. Peter, M. Piacentini, D.C. Rubinsztein, Y. Shi, H.U. Simon, P. Vandenabeele, E. White, J. Yuan, B. Zhivotovsky, G. Melino, G. Kroemer, Molecular definitions of cell death subroutines: recommendations of the Nomenclature Committee on Cell Death 2012, Cell Death Differ. 19 (2012) 107–120.

[3] R.V. Talanian, C. Quinlan, S. Trautz, M.C. Hackett, J.A. Mankovich, D. Banach, T. Ghayur, K.D. Brady, W.W. Wong, Substrate specificities of caspase family proteases, J. Biol. Chem. 272 (1997) 9677–9682.

[4] N.A. Thornberry, T.A. Rano, E.P. Peterson, D.M. Rasper, T. Timkey, M. Garcia-Calvo, V.M. Houtzager, P.A. Nordstrom, S. Roy, J.P. Vaillancourt, K.T. Chapman, D.W. Nicholson, A combinatorial approach defines specificities of members of the caspase family and granzyme B. Functional relationships established for key mediators of apoptosis, J. Biol. Chem. 272 (1997) 17907–17911.

[5] C. Pop, G.S. Salvesen, Human caspases: activation, specificity, and regulation, J. Biol. Chem. 284 (2009) 21777–21781.
[6] K. Schrader, J. Huai, L. Jöckel, C. Oberle, C. Borner, Non-caspase proteases: triggers or amplifiers of apoptosis? Cell. Mol. Life Sci. 67 (2010) 1607–1618.
[7] Y.A. Lazebnik, S.H. Kaufmann, S. Desnoyers, G.G. Poirier, W.C. Earnshaw, Cleavage of poly(ADP-ribose) polymerase by a proteinase with properties like ICE, Nature 371 (1994) 346–347.
[8] Y. Huang, S. Nakada, T. Ishiko, T. Utsugisawa, R. Datta, S. Kharbanda, K. Yoshida, R.V. Talanian, R. Weichselbaum, D. Kufe, Z.M. Yuan, Role for caspase-mediated cleavage of Rad51 in induction of apoptosis by DNA damage, Mol. Cell. Biol. 19 (1999) 2986–2997.
[9] G.C. Smith, F. d'Adda di Fagagna, N.D. Lakin, S.P. Jackson, Cleavage and inactivation of ATM during apoptosis, Mol. Cell. Biol. 19 (1999) 6076–6084.
[10] M.W. Lee, I. Hirai, H.G. Wang, Caspase-3-mediated cleavage of Rad9 during apoptosis, Oncogene 22 (2003) 6340–6346.
[11] C.A. Clarke, L.N. Bennett, P.R. Clarke, Cleavage of claspin by caspase-7 during apoptosis inhibits the Chk1 pathway, J. Biol. Chem. 280 (2005) 35337–35345.
[12] N. Okita, Y. Kudo, S. Tanuma, Checkpoint kinase 1 is cleaved in a caspase-dependent pathway during genotoxic stress-induced apoptosis, Biol. Pharm. Bull. 30 (2007) 359–362.
[13] S. Solier, Y. Pommier, MDC1 cleavage by caspase-3: a novel mechanism for inactivating the DNA damage response during apoptosis, Cancer Res. 71 (2011) 906–913.
[14] S. Mansilla, W. Priebe, J. Portugal, Mitotic catastrophe results in cell death by caspase-dependent and caspase-independent mechanisms, Cell Cycle 5 (2006) 53–60.
[15] K. Matsuura, M. Wakasugi, K. Yamashita, T. Matsunaga, Cleavage-mediated activation of Chk1 during apoptosis, J. Biol. Chem. 283 (2008) 25485–25491.
[16] S. Sidi, T. Sanda, R.D. Kennedy, A.T. Hagen, C.A. Jette, R. Hoffmans, J. Pascual, S. Imamura, S. Kishi, J.F. Amatruda, J.P. Kanki, D.R. Green, A.A. D'Andrea, A.T. Look, Chk1 suppresses a caspase-2 apoptotic response to DNA damage that bypasses p53, Bcl-2, and caspase-3, Cell 133 (2008) 864–877.
[17] K. Myers, M.E. Gagou, P. Zuazua-Villar, R. Rodriguez, M. Meuth, ATR and Chk1 suppress a caspase-3-dependent apoptotic response following DNA replication stress, PLoS Genet. 5 (2009) e1000324.
[18] Y.S. Kaneko, N. Watanabe, H. Morisaki, H. Akita, A. Fujimoto, K. Tominaga, M. Terasawa, A. Tachibana, K. Ikeda, M. Nakanishi, Cell-cycle-dependent and ATM-independent expression of human Chk1 kinase, Oncogene 18 (1999) 3673–3681.
[19] K.L. Rock, C. Gramm, L. Rothstein, K. Clark, R. Stein, L. Dick, D. Hwang, A.L. Goldberg, Inhibitors of the proteasome block the degradation of most cell proteins and the generation of peptides presented on MHC class I molecules, Cell 78 (1994) 761–771.
[20] P. Vandenabeele, S. Orrenius, B. Zhivotovsky, Serine proteases and calpains fulfill important supporting roles in the apoptotic tragedy of the cellular opera, Cell Death Differ. 12 (2005) 1219–1224.
[21] H.J. Rideout, E. Zang, M. Yeasmin, R. Gordon, O. Jabado, D.S. Park, L. Stefanis, Inhibitors of trypsin-like serine proteases prevent DNA damage-induced neuronal death by acting upstream of the mitochondrial checkpoint and of p53 induction, Neuroscience 107 (2001) 339–352.
[22] E.C. de Bruin, D. Meersma, J. de Wilde, I. den Otter, E.M. Schipper, J.P. Medema, L.T. Peltenburg, A serine protease is involved in the initiation of DNA damage-induced apoptosis, Cell Death Differ. 10 (2003) 1204–1212.
[23] L. Cilenti, Y. Lee, S. Hess, S. Srinivasula, K.M. Park, D. Junqueira, H. Davis, J.V. Bonventre, E.S. Alnemri, A.S. Zervos, Characterization of a novel and specific inhibitor for the pro-apoptotic protease Omi/HtrA2, J. Biol. Chem. 278 (2003) 11489–11494.
[24] P. Chen, C. Luo, Y. Deng, K. Ryan, J. Register, S. Margosiak, A. Tempczyk-Russell, B. Nguyen, P. Myers, K. Lundgren, C.C. Kan, P.M. O'Connor, The 1.7 A crystal structure of human cell cycle checkpoint kinase Chk1: implications for Chk1 regulation, Cell 100 (2000) 681–692.
[25] Y. Katsuragi, N. Sagata, Regulation of Chk1 kinase by autoinhibition and ATR-mediated phosphorylation, Mol. Biol. Cell 15 (2004) 1680–1689.
[26] C.P. Ng, H.C. Lee, C.W. Ho, T. Arooz, W.Y. Siu, A. Lau, R.Y. Poon, Differential mode of regulation of the checkpoint kinases CHK1 and CHK2 by their regulatory domains, J. Biol. Chem. 279 (2004) 8808–8819.
[27] M. Walker, E.J. Black, V. Oehler, D.A. Gillespie, M.T. Scott, Chk1 C-terminal regulatory phosphorylation mediates checkpoint activation by de-repression of Chk1 catalytic activity, Oncogene 28 (2009) 2314–2323.
[28] Y.W. Zhang, D.M. Otterness, G.G. Chiang, W. Xie, Y.C. Liu, F. Mercurio, R.T. Abraham, Genotoxic stress targets human Chk1 for degradation by the ubiquitin-proteasome pathway, Mol. Cell 19 (2005) 607–618.
[29] V. Leung-Pineda, J. Huh, H. Piwnica-Worms, DDB1 targets Chk1 to the Cul4 E3 ligase complex in normal cycling cells and in cells experiencing replication stress, Cancer Res. 69 (2009) 2630–2637.
[30] Y.W. Zhang, J. Brognard, C. Coughlin, Z. You, M. Dolled-Filhart, A. Aslanian, G. Manning, R.T. Abraham, T. Hunter, The F box protein Fbx6 regulates Chk1 stability and cellular sensitivity to replication stress, Mol. Cell 35 (2009) 442–453.
[31] M. Tewar, L.T. Quan, K. O'Rourke, S. Desnoyers, Z. Zeng, D.R. Beidler, G.G. Poirier, G.S. Salvesen, V.M. Dixit, Yama/CPP32 beta, a mammalian homolog of CED-3, is a CrmA-inhibitable protease that cleaves the death substrate poly(ADP-ribose) polymerase, Cell 81 (1995) 801–809.
[32] T. Fernandes-Alnemri, A. Takahashi, R. Armstrong, J. Krebs, L. Fritz, K.J. Tomaselli, L. Wang, Z. Yu, C.M. Croce, G.S. Salvesen, W.C. Earnshaw, G. Litwack, E.S. Alnemri, Mch3, a novel human apoptotic cysteine protease highly related to CPP32, Cancer Res. 55 (1995) 6045–6052.
[33] R. Hegde, S.M. Srinivasula, Z. Zhang, R. Wassell, R. Mukattash, L. Cilenti, G. DuBois, Y. Lazebnik, A.S. Zervos, T. Fernandes-Alnemri, E.S. Alnemri, Identification of Omi/HtrA2 as a mitochondrial apoptotic serine protease that disrupts inhibitor of apoptosis protein–caspase interaction, J. Biol. Chem. 277 (2002) 432–438.
[34] N. Katunuma, E. Kominami, Structure, properties, mechanisms, and assays of cysteine protease inhibitors: cystatins and E-64 derivatives, Methods Enzymol. 251 (1995) 382–397.
[35] K. Ishidoh, E. Kominami, Processing and activation of lysosomal proteinases, Biol. Chem. 383 (2002) 1827–1831.
[36] H. Umezawa, Structures and activities of protease inhibitors of microbial origin, Methods Enzymol. 45 (1976) 678–695.
[37] M.N. Greco, M.J. Hawkins, E.T. Powell, H.R. Almond HR Jr., T.W. Corcoran, L. de Garavilla, J.A. Kauffman, R. Recacha, D. Chattopadhyay, P. Andrade-Gordon, B.E. Maryanoff, Nonpeptide inhibitors of cathepsin G: optimization of a novel beta-ketophosphonic acid lead by structure-based drug design, J. Am. Chem. Soc. 124 (2002) 3810–3811.
[38] S. Conus, H.U. Simon, Cathepsins: key modulators of cell death and inflammatory responses, Biochem. Pharmacol. 76 (2008) 1374–1382.
[39] J. Tözsér, P. Bagossi, G. Zahuczky, S.I. Specht, E. Majerova, T.D. Copeland, Effect of caspase cleavage-site phosphorylation on proteolysis, Biochem. J. 372 (2003) 137–143.

AGE (2013) 35:1143–1156
DOI 10.1007/s11357-012-9439-1

Caloric restriction-associated remodeling of rat white adipose tissue: effects on the growth hormone/insulin-like growth factor-1 axis, sterol regulatory element binding protein-1, and macrophage infiltration

Yoshikazu Chujo · Namiki Fujii · Naoyuki Okita · Tomokazu Konishi · Takumi Narita · Atsushi Yamada · Yushi Haruyama · Kosuke Tashiro · Takuya Chiba · Isao Shimokawa · Yoshikazu Higami

Received: 27 December 2011 / Accepted: 16 May 2012 / Published online: 28 May 2012

Abstract The role of the growth hormone (GH)-insulin-like growth factor (IGF)-1 axis in the lifelong caloric restriction (CR)-associated remodeling of white adipose tissue (WAT), adipocyte size, and gene expression profiles was explored in this study. We analyzed the WAT morphology of 6–7-month-old wild-type Wistar rats fed ad libitum (WdAL) or subjected to CR (WdCR), and of heterozygous transgenic dwarf rats bearing an anti-sense GH transgene fed ad libitum (TgAL) or subjected to CR (TgCR). Although less effective in TgAL, the adipocyte size was significantly reduced in WdCR compared with WdAL. This CR effect was blunted in Tg rats. We also used high-density oligonucleotide microarrays to examine the gene expression profile of WAT of WdAL, WdCR, and TgAL rats. The gene expression profile of WdCR, but not TgAL, differed greatly from that of WdAL. The gene clusters with the largest changes induced by CR but not by Tg were genes involved in lipid biosynthesis and inflammation, particularly sterol regulatory element binding proteins (SREBPs)-regulated and macrophage-related genes, respectively. Real-time reverse-transcription polymerase chain reaction analysis confirmed that the expression of *SREBP-1* and its downstream targets was upregulated, whereas the macrophage-related genes were downregulated in WdCR, but not in TgAL. In addition, CR affected the gene expression profile of Tg rats similarly to wild-type rats. Our findings suggest that CR-associated remodeling of WAT, which involves SREBP-1-mediated transcriptional activation and suppression of macrophage infiltration, is regulated in a GH–IGF-1-independent manner.

Yoshikazu Chujo, Namiki Fujii, Naoyuki Okita, and Tomokazu Konishi contributed equally to this work.

Electronic supplementary material The online version of this article (doi:10.1007/s11357-012-9439-1) contains supplementary material, which is available to authorized users.

Y. Chujo · N. Fujii · N. Okita · T. Narita · A. Yamada · Y. Haruyama · Y. Higami (✉)
Molecular Pathology and Metabolic Disease, Faculty of Pharmaceutical Sciences, Tokyo University of Science, Chiba, Japan
e-mail: higami@rs.noda.tus.ac.jp

T. Konishi
Molecular Genetics Group, Akita Prefectural University, Akita, Japan

K. Tashiro
Graduate School of Bioresource and Bioenvironmental Sciences, Molecular Gene Technics, Kyushu University, Fukuoka, Japan

T. Chiba · I. Shimokawa
Department of Investigative Pathology, Nagasaki University Graduate School of Biomedical Sciences, Nagasaki, Japan

Keywords Growth hormone · Insulin-like growth factor-1 · Caloric restriction (CR) · Lipid biosynthesis · Sterol regulatory element binding protein · DNA microarray

Introduction

Ames and Snell mutant dwarf mice, which lack growth hormone (GH), prolactin, and thyroid-stimulating hormone, live approximately 20–50 % longer than wild-type mice (Brown-Borg et al. 1996; Flurkey et al. 2001). Similarly, disrupted GH receptor/binding protein (GHR/BP) knockout (KO) mice live significantly longer than their wild-type controls (Coschigano et al. 2000). The longevity of heterozygous insulin-like growth factor (IGF)-1 receptor KO mice, and both heterozygous and homozygous insulin receptor substrate-1 KO mice (particularly females) show markedly extended lifespan compared with their counterparts (Holzenberger et al. 2003). We have also reported that heterozygous transgenic dwarf rats, bearing an anti-sense GH transgene, live longer than controls (Shimokawa et al. 2002). Based on these studies, the GH–IGF-1 axis and/or its related signaling pathways are important lifespan regulators (Bartke 2005).

Although new genetic interventions that extend the lifespan of mammals are emerging, caloric restriction (CR) remains the most robust, reproducible, and simple experimental manipulation known to extend both median and maximum lifespan, and to delay the onset of many age-associated pathophysiological changes in laboratory rodents (Weindruch and Walford 1988; Yu 1994). In general, attenuation of oxidative and other stresses, the modulation of glycemia and insulinemia, and the activation of sirtuin may be significant factors in the beneficial effects of CR (Weindruch and Walford 1988; Yu 1994; Sohal and Weindruch 1996; Masoro 2005; Sinclair 2005). Moreover, Nisoli et al. (2005) suggested that the enhanced mitochondrial biogenesis is also involved in the beneficial action of CR. Thereafter, several investigators reported that CR induces mitochondrial biogenesis (Anderson and Prolla 2009; López-Lluch et al. 2006; Shi et al., 2005). On the other hand, Hancock et al. (2011) and Gesing et al. (2011) demonstrated that CR does not increase it. Recently, we also reported that CR enhances mitochondrial biogenesis in white adipose tissue (WAT) but not in brown adipose tissue (Okita et al. 2012). Thus, the exact mechanisms underlying CR are still debated. CR animals share many characteristics with long-living dwarf mice, including smaller body size, and lower plasma insulin and IGF-1 levels (Sinclair 2005; Al-Regaiey et al. 2005). CR does not further extend the lifespan of the already long-lived GHR/BP KO mice (Bonkowski et al. 2006). In contrast, CR further extends the longevity of Ames dwarf mice and heterozygous transgenic dwarf rats bearing an anti-sense GH transgene, which live longer than their wild-type controls (Bartke et al. 2001; Shimokawa et al. 2003). Therefore, the beneficial effects of CR are not solely dependent on the GH–IGF-1 axis. In terms of the hepatic gene expression profile, CR mainly alters the expression of genes involved in the stress response, xenobiotic metabolism, and lipid metabolism. Most genes involved in stress response and xenobiotic metabolism are regulated in a GH–IGF-1-dependent manner, while those involved in lipid metabolism are regulated in a GH–IGF-1-independent manner. Moreover, CR enhances the expression of genes involved in fatty acid synthesis after feeding, and of genes encoding mitochondrial β-oxidation enzymes during food shortage, probably via transcriptional regulation by sterol regulatory element binding protein 1 (SREBP-1) and peroxisome proliferator-activated receptor (PPAR)-α, respectively (Higami et al. 2006b). Considering these findings together with serum biochemical parameters, we proposed that CR enhances lipid utilization via hepatic transcriptional changes and prevents hepatic steatosis in a GH–IGF-1-independent manner (Higami et al. 2006b).

Adipose tissue plays a central role in the regulation of both energy storage and expenditure (Saely et al. 2012). Numerous WAT-derived secretory molecules, including leptin, tumor necrosis factor (TNF)-α, and adiponectin, have been characterized, and some of these molecules play significant roles in obesity and insulin resistance (Torres-Leal et al. 2010; Ouchi et al. 2011). Therefore, WAT is now recognized as an endocrine organ rather than an inert tissue, and is implicated in the pathogenesis and complications of type 2 diabetes. It has been reported that fat-specific insulin receptor knockout mice live longer than their controls (Blüher et al. 2003). These mice show reduced adiposity and altered secretion of adipokines, including higher adiponectin and lower pro-inflammatory cytokine levels (Blüher et al. 2002). The transcription factors C/EBPα, C/EBPβ, and PPARγ are master regulators of adipocyte differentiation (Farmer 2006). Mice in which C/EBPα is replaced with C/EBPβ (β/β

mice) live longer and have reduced adiposity compared with their wild-type controls (Chiu et al. 2004). In contrast, hetero-deficient PPARγ KO mice have a shortened lifespan (Argmann et al. 2009). Transgenic mice expressing adiponectin in the liver live longer than controls, and are resistant to high-calorie diet-induced obesity (Otabe et al. 2007). Thus, altered adipose tissue gene expression and modulation of adipokine secretion seem to influence the lifespan of rodents. CR reduces adiposity and reduces adipocyte size by altering the gene expression profile (Higami et al. 2004, 2006a). CR decreases plasma insulin and leptin levels, and increases plasma adiponectin levels (Higami et al. 2005; Yamaza et al. 2007). CR also reverses age-associated insulin resistance, possibly by decreasing adiposity (Barzilai et al. 1998). Moreover, Masternak et al. (2012) reported that visceral fat removal improved insulin sensitivity, suppressed fat accumulation in the skeletal muscle, and reduced body temperature and respiratory quotient in wild-type mice and had opposite effects on long-living GHR/BP KO mice. Therefore, we hypothesized that the beneficial actions of CR may be partially mediated by WAT remodeling as well as decreasing adiposity.

In the present study, to explore the role of the GH–IGF-1 axis in CR-associated remodeling of WAT, we compared adipocyte size and gene expression profiles of WAT between CR rats and transgenic dwarf rats, bearing an anti-sense GH transgene. We propose that CR-associated remodeling of WAT, which is transcriptionally regulated by SREBP-1 and modulated by macrophage infiltration, could be regulated in a GH–IGF-1-independent manner.

Materials and Methods

Animals

The present study was conducted in accordance with the provisions of the Ethics Review Committee for Animal Experimentation at Nagasaki University. The rat characteristics and animal care are described elsewhere (Higami et al. 2006a). Briefly, in this study we used ad libitum (AL)-fed male heterozygous transgenic dwarf rats, bearing the anti-sense growth hormone transgene (tg/−; Tg), and their genetic background, Jcl:Wistar (−/−; wild-type) rats. From 6 weeks of age, both wild-type and Tg rats were divided into two groups: AL and CR (70 % of the energy intake). CR was started without adjustment for food shortage. CR rats were fed every other day. Their 2-day food allotment was equal to 140 % of the mean daily intake of AL rats. Wild-type AL (WdAL) and CR (WdCR), and Tg AL (TgAL) and CR (TgCR) rats were killed at 6–7 months of age. The day before the rats were killed, they were all provided with their allocated food 30 min before the lights were turned off in the evening and were killed after the lights were turned on the following morning. Thus, all rats were not under fasting condition when killed. Immediately after killing the rats, epididymal white adipose tissue (WAT) was collected and its weight was measured. Some of the isolated WAT was fixed in a buffered formalin solution for histological examination and the rest was immediately diced, frozen in liquid nitrogen, and stored at −80°C. Total RNA was extracted from the stored WAT for DNA microarray analysis and quantitative real-time reverse-transcription polymerase chain reaction (RT-PCR).

Histological examination

Fixed tissues were processed routinely and embedded in paraffin. Tissue sections (5 μm thick) were stained with hematoxylin–eosin. The stained sections were scanned by microscopy with a charge-coupled device camera (Nikon, Tokyo, Japan). All images were recorded after precise focusing. ImageJ 1.43u/Java1.6.0_22 software was used for all tissue analyses. The size distribution of each white area in the black-and-white images, corresponding to lipid droplets, was counted and calculated. To avoid inter-rater variation, a single observer (YC) carried out tissue analyses.

Microarrays and data normalization

Total RNA was measured using an Affymetrix Rat Genome 230_2.0 GeneChip (Affymetrix, Santa Clara, CA, USA), with four biological repeats per group. The raw data were deposited in Gene Expression Omnibus (accession code: GSE30668). The perfect match data were normalized and the expression levels of each gene were estimated using the SuperNORM data service (Skylight Biotech Inc., Akita, Japan) according to a three-parameter log-normal distribution model (Konishi et al. 2008). To reduce noise effects, the analyses were focused on genes identified as positive by two-way analysis of variance (ANOVA), with a two-sided threshold of 0.001. Out of 31,099 genes on each chip, 6,641 were positive.

Principal component analysis

To compare the effects of CR (WdAL vs. WdCR) with those of Tg (WdAL vs. TgAL), we performed principal component (PC) analysis (Jackson 2005) on the ANOVA-positive genes. To reduce the effects of individual differences between samples, the axes of the PC analysis were estimated on a matrix of each group's sample means and applied to all data, which were centered using the sample means of WdAL rats (the R scripts used are available in the Supplemental Materials and Methods). The methodology rotated the original data matrix around the center of the WdAL rats, to fit perpendicular axes toward which most of the variations in the data appeared. The distribution of each PC value was checked on a normal QQ plot and outlier genes that departed from the normality (PC1: >0.16 and < –016 in Supplemental Fig. 1; PC2: >0.1 and < –0.1 in Supplemental Fig. 2) were selected.

Evaluation of frequently occurring biological functions in gene annotations

To test the significance among categories of biological functions that appeared in the selected genes' annotations, we applied binomial statistical tests based on the frequencies found in the Gene Ontology (GO) Biological Process annotations (release 31) provided by Affymetrix (Konishi et al. 2008).

Quantitative real-time RT-PCR

To obtain cDNA, 1 μg of RNA extracted from WAT of WdAL, WdCR, TgAL, and TgCR rats was reverse transcribed using PrimeScript Reverse Transcriptase (Takara, Shiga, Japan) with random hexamers (Takara). Quantitative real-time PCR was performed using an Applied Biosystems 7300 real-time PCR system (Applied Biosystems, Carlsbad, CA, USA) with SYBR Premix ExTaqII (Takara). The primer sequences for *SREBP-1a*, *SREBP-1c*, *SREBP-2*, *fatty acid synthase* (*FASN*), *acetyl-CoA carboxylase 1* (*ACC1*), *squalene epoxidase* (*Sqle*), *mevalonate kinase* (*Mvk*), *F4/80*, *monocyte chemotactic protein-1* (*MCP-1*), *CD11c* (also known as *integrin alpha X*), *CD163*, and *TATA box binding protein* (*TBP*) are shown in Table 1. TBP was used as a normalization control. The amount of target mRNA relative to *TBP* mRNA in the three groups was obtained. Data from three to six rats per group are expressed as means±SEM and were compared using Tukey's *t* test. Differences were considered statistically significant at $P<0.05$.

Results

CR markedly reduced the body weight of both wild-type and Tg rats. Tg also significantly decreased the body weight of both AL and CR rats (WdAL, 486.9± 29.9 g; WdCR, 349.7±15.6 g; TgAL, 310.3±12.1 g; TgCR, 237.8±25.7 g). Similarly, CR markedly reduced the epididymal WAT weight of both wild-type and Tg rats. Tg also significantly reduced it in both AL and CR rats (WdAL, 7.02±1.04 g; WdCR, 4.96± 0.97 g; TgAL, 4.76±0.74 g; TgCR, 4.32±0.88 g). In contrast, WAT weight as a percentage of body weight, which represents adiposity, did not differ among WdAL, WdCR, and TgAL rats, but it was markedly increased in TgCR rats (WdAL, 1.44± 0.18 %; WdCR, 1.42±0.27 %; TgAL, 1.53± 0.22 %; TgCR, 1.81±0.26 %).

CR significantly reduced the size of white adipocytes, but this effect was predominantly found in wild-type rats compared with Tg rats (Fig. 1a–d). Tg also slightly reduced their size, but it was likely that the effect of Tg was less than that of CR (Fig. 1a and c). In fact, the median adipocyte size was significantly smaller in WdCR than in WdAL, but not in TgCR compared with TgAL. It was slightly but significantly smaller in TgAL than in WdAL (WdAL vs. WdCR: $p=0.001$, TgAL vs. TgCR: $p=0.100$, WdAL vs. TgAL: $p=0.026$, Fig. 1f). The percentage of adipocytes showing >5,000 μm^2 was also significantly lower in WdCR than WdAL, but not in TgCR compared with TgAL. It was slightly but significantly smaller in TgAL than in WdAL (WdAL vs. WdCR: $p<0.001$, TgAL vs. TgCR: $p=0.090$, WdAL vs. TgAL: $p=0.039$, Fig. 1g). In WAT of WdCR and TgCR, the adipocytes were predominantly 1,000–3,000 μm^2 in area, whereas those in WdAL and TgAL WAT showed a much greater size distribution. This pattern was more significant in WdAL than in TgAL rats (Fig. 1e).

Based on the DNA microarray data of WdAL, WdCR, and TgAL, using high-density oligonucleotide microarrays, 6,641 genes were positive based on two-way ANOVA ($P<0.001$). These genes were applied to PC analysis. The PC scores for each group and their